USING MULTIBODY DYNAMICS FOR THE STABILITY ASSESSMENT OF A NEW DOUBLE-SWEPT ROTOR BLADE SETUP

Jürgen Arnold, Juergen.Arnold@dlr.de, DLR German Aerospace Center

Stefan Waitz, Stefan.Waitz@dlr.de, DLR German Aerospace Center

Abstract

A new double-swept rotor blade setup has been assessed in frequency domain for both, dynamic stability in terms of ground resonance and aeroelastic stability related to rotor blade and rotor flutter. The blade setup is being developed for a rotor test rig and will be operated under axial inflow. Methodology is based on a multibody system which is coupled with an unsteady aerodynamic model based on Wagner's function and related enhancements for the general motion of an airfoil section considering heave and pitch motion. The simulation model uses modelling techniques for the setup of a linearized model and allows both, the investigation of ground resonance and flutter for the rig with clamped and articulated rotor blades in frequency domain. Numerical results for the two- and four-bladed rotor state dynamic stability for the setup with clamped blades within the planned rotor speed range up to 65 Hz, whilst the setup using articulated blades with lead-lag hinges indicates instability at low scale starting from a rotor frequency of 30 Hz. The aeroelastic assessment shows a small hump in the damping curves for the two-bladed rotor which is found instable at rotor speeds around 20 Hz for both rotor setups. Here, the flutter mechanism has major contributions from the backward whirl mode and flap bending modes. In contrast, the four-bladed rotor configurations do not show flutter.

1. INTRODUCTION

With the "Rotor Test Stand Göttingen (RTG)" a new test rig has been developed in the DLR Institute of Aerodynamics and Flow Technology [1] for the physical investigation of dynamic stall phenomena. To support the secure entry into service numerous simulations using multibody dynamics have been performed in the DLR Institute of Aeroelasticity to assess both, the dynamic stability in terms of ground resonance and aeroelastic stability related to rotor blade or rotor flutter. An earlier ERF contribution [2] dealt with the RTG test rig itself that has been so far operated with conventional, straight rotor blades in two- and four-bladed configurations as shown in Figure 1.

Copyright Statement
The authors confirm that they, and/or their company or organization, hold *copyright on all of the original material included in this paper. The authors also confirm that they have obtained permission, from the copyright holder of any third party material included in this paper, to publish it as part of their paper. The authors confirm that they give permission, or have obtained permission from the copyright holder of this paper, for the publication and distribution of this paper as part of the ERF proceedings or as individual offprints from the proceedings and for inclusion in a freely accessible web-based repository*.

Focus of this paper is now on the stability assessment of an innovative rotor blade layout with forward and backward sweep that is currently prepared and depicted in Figure 2. Since the overall objective, the used methodology and the basic model of the RTG test rig remain unchanged, parts of this earlier contribution are used and extended for the new rotor blade setup.

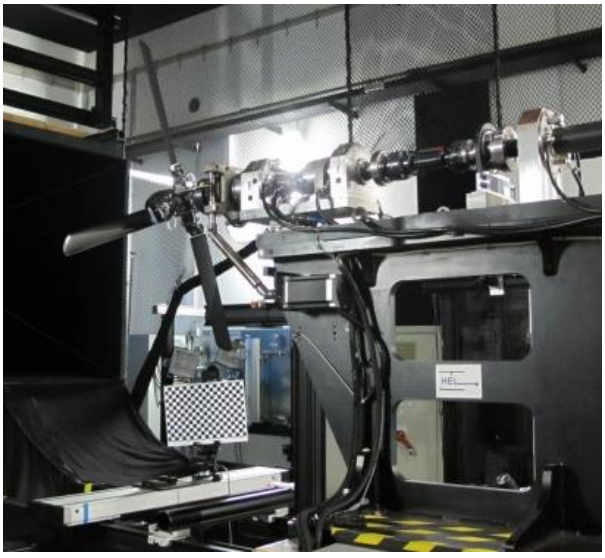

Figure 1: RTG test rig with conventional rotor blades.

Presented at 44th European Rotorcraft Forum, Delft, The Netherlands, 19-20 September, 2018
This work is licensed under the Creative Commons Attribution International License (CC BY). Copyright © 2018 by author(s).

Major improvement of the overall prediction capability for dynamic and aeroelastic simulation of rotorcraft is available by means of a multibody system (MBS) for the setup of the mechanical model [3]-[4] which is characterized by connected rotary and non-rotary substructures. The application of multibody dynamics allows the consideration of all non-linear contributions relevant in a rotating system like geometric stiffening of the flexible blades and additional damping terms activated by gyroscopic effects as well as the provision of a correct mechanical interface between the rotating and non-rotating frames by applying non-linear joint definitions. Here, the multibody system SIMPACK [5]-[6] is used for the setup and simulation of the mechanical model of the rotor in a two- and four-bladed configuration with its flexible blades. Flexibility of the non-rotating blade is described in the multibody system SIMPACK with a modal approach for available finite element models. For the assessment of the rotor in axial inflow condition, an unsteady theory using indicial aerodynamics based on Wagner's function [7] in combination with steady two-dimensional airfoil data is applied to the multibody model.

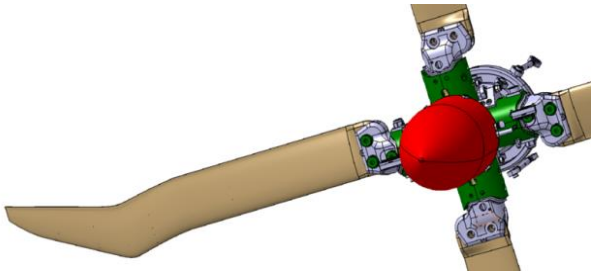

Figure 2: RTG double-swept rotor blade.

The paper addresses a discussion of used techniques to obtain a linearized model of the rig with clamped and articulated rotor blades allowing the straight-forward assessment in frequency domain, an overview about the performed stability analyses and finally, a comparison of the investigated stability behavior for the two- and four-bladed RTG rotor configurations with the new double-swept blades. The presented work is based on results from the current DLR FAST-Rescue project.

2. NUMERICAL METHODS

2.1. Multibody Dynamics

The multibody system SIMPACK [5]-[6] is used to set up and simulate the mechanical model of the rotor system with its flexible rotor blades including large rigid body motions of the rotor hub and blade hinges as well as small deformations of the elastic structure. The development of the simulation package was originally initiated by DLR and later out-sourced for further development and commercial distribution. It provides all non-linear inertial coupling terms and allows the setup of elastic simulation models.

Flexibility of the non-rotating blade is described in the multibody system SIMPACK with a modal approach [8]-[9] for available finite element models. Several features allow the introduction of elastic rotor blades:

(A) Implementation of complete elastic blade as one elastic body and additional geometric stiffness terms via standard FlexModal interface

(B) Implementation of elastic blade with connected elastic substructures via standard FlexModal interface

(C) Application of the intrinsic elastic beam model SIMBEAM

(D) Application of the Rotor Blade Generator based on SIMBEAM

Feature (A) allows the straight-forward use of finite element models of industrial model size. Currently, the FlexModal interface supports ABAQUS, ANSYS, I-DEAS, MSC.NASTRAN, NX.NASTRAN and PERMAS. The feature (B) might be advantageous to add further non-linear characteristics of the multibody joints that interconnect elastic substructures. Feature (C) and (D) provide a solution, if a finite element code is not available or is not supported by FlexModal. In the present work, SIMPACK version 9.92 has been used.

Feature (A) which is based on the implementation of the complete elastic model together with additional geometric stiffness using the FlexModal interface is chosen for the RTG rotor blades. Two FEM solutions from a preprocessing step with the finite element code ANSYS are required in order to process the blade:

- A modal solution provides the modal elastic model with natural frequencies and mode shapes for the non-rotating blade at Ω=0 Hz.
- A static solution provides the geometric stiffness terms for the description in the relevant degrees-of-freedom of the rotating blade for Ω>0 Hz (centrifugal forces due to angular velocity).

FlexModal reads the model geometry, mass and stiffness matrices, natural frequencies, mode shapes, geometric stiffening terms and the used

Presented at 44th European Rotorcraft Forum, Delft, The Netherlands, 19-20 September, 2018
This work is licensed under the Creative Commons Attribution International License (CC BY). Copyright © 2018 by author(s).

load case entries for the derivation of the geometric stiffening terms from the pre-processed finite element data. Then, FlexModal translates this input into a common flexibility description which is based on the Standard Input Data (SID) format as described in [9]. The file containing the flexible substructure is added in SIMPACK with marker locations which are the same as found at the node positions in the finite element model, changing a rigid into an elastic body. Regarding aspects of component modal synthesis and substructuring, any hybrid model consisting of rigid and flexible bodies can be built. Rigid bodies can be made flexible by the introduction of a modal elastic model as described above or spring stiffness can be applied to a joint between two bodies from the MBS element library. SIMPACK adds the additional equations for the modal degrees-of-freedom to the set of differential algebraic equations (DAE) and solves the resulting set of equations.

2.2. Indicial Aerodynamics

The used unsteady aerodynamic model is based on indicial functions for circulatory terms and apparent mass terms for non-circulatory effects. Two important formulations of unsteady aerodynamic force models in the time domain [7] go back to H. Wagner (pulse in angle of attack of airfoil section / application to flutter problem) and H.G. Küssner (local change of inflow for airfoil / application to gust problem). Both models are realized in MBS SIMPACK with a User Force Element (UFEL). They describe the motion induced velocities on the airfoil and the continuous immersion of the profile cross-section in the interference of a gust, respectively. Here, aerodynamics using Wagner's function [10] is applied to the multibody model. The fast aerodynamic model based on radial independent strips has been used to study basic phenomena of different blade layouts [11] and setups of the RTG rotor test rig.

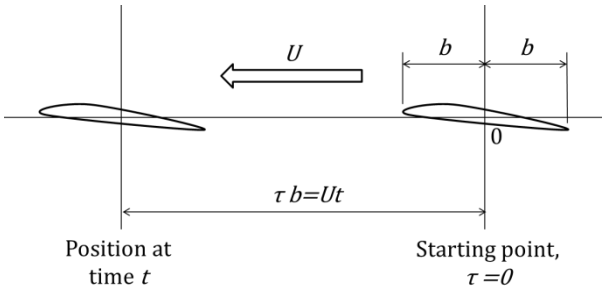

Figure 3: Impulsive motion of an airfoil.

Wagner considers a two-dimensional thin airfoil of chord length $2b$ in an impulsive motion from rest to the uniform velocity U and is commonly used as a model to describe the unsteady lift development for a change in angle-of-attack. This motion is depicted in Figure 3 for distance τ traveled in semichords during time t.

The lift due to circulation acting on the strip of unit span [7] follows for an incompressible fluid of density ρ and the downwash w as

$$L_1 = 2\pi b \rho U w \Phi(\tau), \qquad \tau = Ut/b \tag{1}$$

where $\Phi(\tau) = 1 - 0.165e^{-0.0455\tau} - 0.335e^{-0.300\tau}$

represents the approximation of R.T. Jones for Wagner's function $\Phi(\tau)$ describing the unsteady lift development towards the steady-state value for increasing distance τ traveled in semichords b. The approximation is shown in Figure 4 together with values generated from the state-space formulation of Wagner's function in the SIMPACK User Force Element [12]-[13].

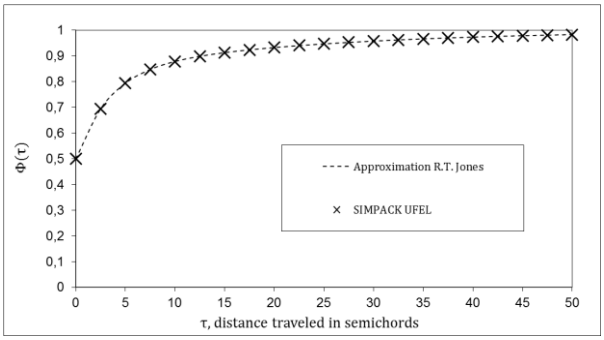

Figure 4: Wagner's function for an incompressible fluid.

According to Y.C. Fung [7], the description of unsteady lift can be extended from an impulsive to a general motion which is illustrated in Figure 5. It includes both, pitch motion α around the elastic axis at $a_h b$ and heave motion h. In this case one part of the lift arises from circulation, and the other part from non-circulatory "apparent mass" forces.

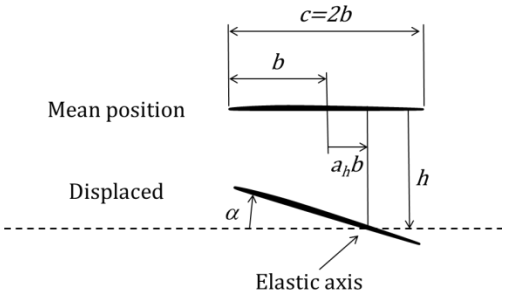

Figure 5: General motion of a two-dimensional airfoil.

Presented at 44th European Rotorcraft Forum, Delft, The Netherlands, 19-20 September, 2018
This work is licensed under the Creative Commons Attribution International License (CC BY). Copyright © 2018 by author(s).

To obtain the circulatory lift for the general motion, the measurement of downwash w in heave direction has to be changed from the ¼ chord point to the Pistolesi point at ¾ chord. Here, the quasi-steady downwash of a two-dimensional airfoil undergoing an arbitrary pitch and heave motion around quarter chord [14] is given by:

$$w = \alpha U + \dot{\alpha} b + \dot{h} \tag{2}$$

The additional non-circulatory contributions to lift and moment from apparent mass $\rho\pi b^2$ and apparent moment of inertia $\rho\pi b^2(b^2/8)$ must be added for the general motion:

$$L_2 = \rho\pi b^2\left(\ddot{h} - a_h b\ddot{\alpha}\right) \tag{3}$$

$$L_3 = \rho\pi b^2 U\dot{\alpha} \tag{4}$$

$$M_a = -\frac{\rho\pi b^4}{8}\ddot{\alpha} \tag{5}$$

Hence, total unsteady lift L and moment M about the elastic axis at $a_h b$, both given per unit span follow as:

$$L = L_1 + L_2 + L_3 \tag{6}$$

$$M = \left(\frac{1}{2} + a_h\right) bL_1 + a_h bL_2 - \left(\frac{1}{2} - a_h\right) bL_3 + M_a \tag{7}$$

The lift amplitude and phase obtained for the implemented SIMPACK User Force Element from a harmonic oscillation in angle-of-attack with angular velocity ω are shown in Figure 6 versus the reduced frequency k which is defined as:

$$k = \omega b/U \tag{8}$$

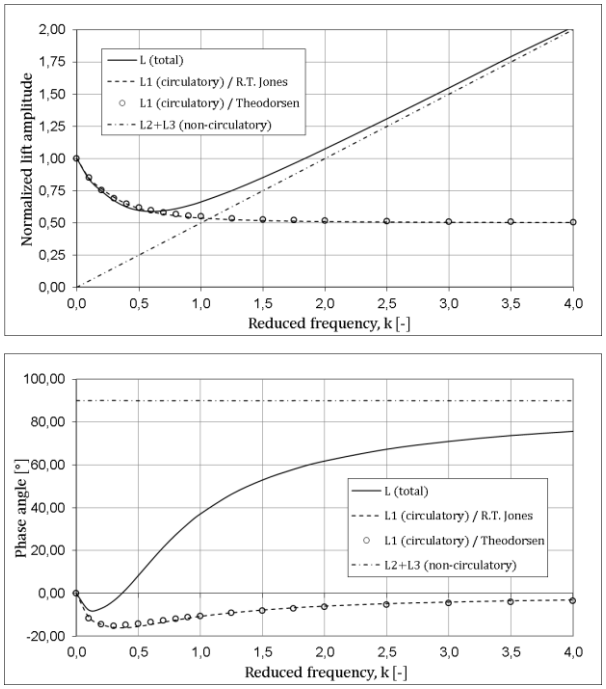

Figure 6: Lift amplitude and phase for circulatory and non-circulatory terms in angle-of-attack oscillation.

Here, the contribution from the circulatory term L_1 is compared to values gained from Theodorsen's function [7]. In general, the results agree very well for amplitude, but show deviations for phase angle at reduced frequencies around 0.5. Further, the contributions from non-circulatory terms L_2 and L_3 as well as the total lift L closely match the values found in literature [15].

The total values for lift and moment hold for a two-dimensional flow of an incompressible fluid. All contributions are implemented in the used SIMPACK User Force Element and resulting forces and moments account for compressibility through Mach number correction. The temporal evolution of lift from Wagner's impulsive motion is described by a differential equation of 2nd order for 2 lag states and is numerically solved in state-space. This allows the consideration of unsteady contributions in time domain and in terms of aerodynamic lag states in frequency domain. Beside the unsteady aerodynamic forces based on Wagner's function and apparent mass, the SIMPACK User Force Element uses stripwise airfoil data based on quasi-steady derivatives and coefficients to account for the steady values of lift, drag and moment. The input is derived from CFD computations of the radially distributed two-dimensional airfoil sections [1].

2.3. Stability Assessment of Dynamic and Aeroelastic Rotor System

Standard features in the multibody system allow the dynamic as well as the aeroelastic assessment of the rotor for axial inflow condition in both, frequency and time domain. Further, the evaluation of the aeroelastic system is performed in a tightly-coupled manner on the MBS level. In the case of RTG, numerical simulations in the frequency domain are used to study the dynamic and aeroelastic stability w.r.t. ground resonance as well as rotor blade and rotor flutter. The approach in frequency domain which is based on linearization, consecutive analysis of the eigenbehaviour and stability rating from damping values can be followed here, since the system matrices for the symmetric rotor with axial inflow remain time invariant and the unsteady aerodynamic forces are considered in terms of aerodynamic lag states.

3. MODELS AND RESULTS

3.1. Dynamic and Aerodynamic Simulation Models

A two- and four-bladed configuration of the rotor test rig with the double-swept blades will be operated and need to be assessed to proof a

Presented at 44th European Rotorcraft Forum, Delft, The Netherlands, 19-20 September, 2018
This work is licensed under the Creative Commons Attribution International License (CC BY). Copyright © 2018 by author(s).

stable running behaviour before the entry into service. Used input for the model setup comprises mass and inertia data from CATIA, the ANSYS finite element model of the elastic rotor blade and modal measurements from a ground vibration test (GVT) on the rig itself. The mechanical setup of the four-bladed RTG rotor system in SIMPACK is depicted in Figure 7 and consists of the flexible rotor blades and the rigid bodies for the drive shaft, rotor hub, pitch bearings and blade hinges.

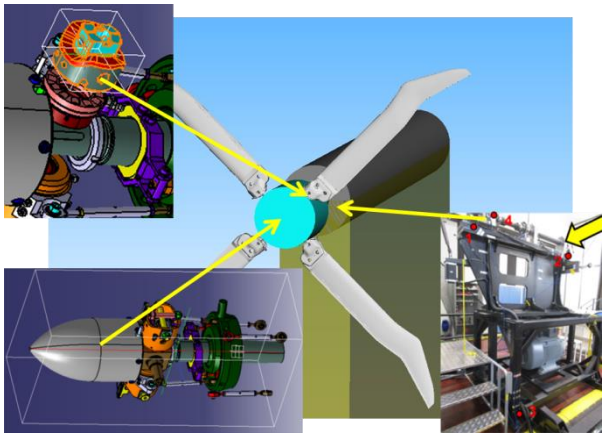

Figure 7. Multibody model of RTG rotor test rig in four-bladed configuration.

All the substructures of the rotor system are modelled with SIMPACK features. The flexibility of the non-rotating blade is described in the multibody system with a modal approach from a real modes solution and additional geometric stiffness contributions for the rotating blade which are considered by static load cases for the relevant degrees of freedom (rotation, flap), both computed in a pre-processing step with the finite element software ANSYS [16]. All studied rotor configurations use identical rotor blades with a blade tip radius of 0.652 m and a reference blade chord of 0.072 m. Available flap and lead-lag hinges are located at the radius of 0.085 m and 0.100 m, respectively. The blade attachment is found at the radial station of 0.131 m and the blade mass is around 0.27 kg. Eigenfrequencies of the non-rotating rotor blade in clamped boundary condition are given in Table 1.

The description of the elastic attachment for the rotor hub resulting from motion contributions of the test rig and the drive shaft is implemented with the equivalent simplified model of measured shaft modes. Here, the elastically mounted RTG rotor is modelled with a fictitious shaft (cardan) joint as depicted in Figure 8 that is adjusted to the measured modal data in terms of eigen-frequencies and mode shapes. As location of the cardan joint the position of the first nodal point of the respective elastic eigenmode of the shaft had been chosen. The applied joint stiffness has been selected in accordance to the respective shaft bending eigenfrequency of 113.17 Hz as identified in GVT. The resulting shaft stiffness is isotropic and enables the used approach for stability assessment also for the two-bladed rotor.

Mode No.	0 Hz Rotor Speed
1	F1 / 43.81 Hz
2	F2 / 177.14 Hz
3	L1 / 242.08 Hz
4	T1 / 316.26 Hz
5	F3 / 455.85 Hz
(F = flap mode / L = lag mode / T = torsion mode)	

Table 1: Eigenfrequencies of the clamped rotor blade.

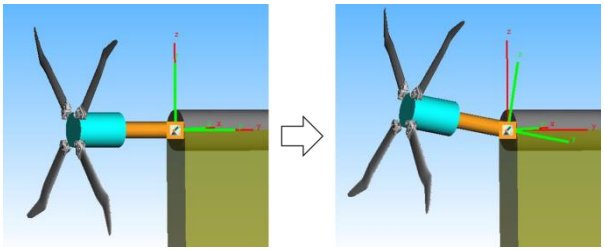

Figure 8. Elastically mounted RTG rotor using a fictitious shaft (cardan) joint.

Along the straight blade axis and the forward-backward swept tip section a total number of 51 User Force Elements are distributed at quarter chord. They provide the unsteady aerodynamic forces based on Wagner's function and related enhancements for the general motion of the airfoil section taking heave and pitch into account. Further, a constant axial inflow of 10 m/s is given for the RTG which is operated downstream in the jet of a wind tunnel nozzle [1]. At the blade tip, a Mach number of 0.60 is reached for the nominal rotor speed of 50 Hz.

3.2. Dynamic Simulation Results

The dynamic properties of the non-rotating two-bladed rotor include a pairwise appearance of symmetric and antisymmetric eigenforms of the elastic rotor blades (named: sym / anti) and two whirl modes which exhibit a coupled motion of the rotor blades together with the elastically mounted rotor hub. With rotation, the eigenforms of the elastic rotor blades exhibit an increase in the natural frequencies, whilst the whirl modes show a characteristic increase and decrease of their

Presented at 44th European Rotorcraft Forum, Delft, The Netherlands, 19-20 September, 2018
This work is licensed under the Creative Commons Attribution International License (CC BY). Copyright © 2018 by author(s).

natural frequencies in terms of a so-called forward and backward whirl (named: W-fwd / W-bwd) as a function of the rotational speed. According values are found in Table 2. Here, it can clearly be seen that the whirl modes change their frequencies by approximately 50 Hz between the non-rotating case and at the nominal rotor speed of 50 Hz. Additional rotational springs with an equivalent stiffness value had been added at each hub shaft in order to account for the elasticity of the rotor head itself. As a result the lead-lag frequency of around 96.15 Hz from the detailed finite element model of the elastic rotor hub and straight blade [17] in clamped boundary condition is obtained at zero rotation.

Mode No.	0 Hz Rotor Speed	50 Hz Rotor Speed
1	F1-anti / 43.77 Hz	F1-anti / 70.79 Hz
2	F1-sym / 43.81 Hz	F1-sym / 70.79 Hz
3	W-bwd / 77.37 Hz	W-bwd / 28.21 Hz
4	W-fwd / 78.31 Hz	W-fwd / 128.52 Hz
5	L1-anti / 99.60 Hz	L1-anti / 103.26 Hz
6	L1-sym / 101.56 Hz	L1-sym / 104.35 Hz
7	F2-sym / 179.59 Hz	F2-sym / 215.57 Hz
8	F2-anti / 179.64 Hz	F2-anti / 215.61Hz
9	T1-sym / 314.21 Hz	T1-sym / 329.95 Hz
10	T1-anti / 314.24 Hz	T1-anti / 329.98 Hz
(F = flap mode / L = lag mode / T = torsion mode / W = whirl)		

Table 2: Natural frequencies of two-bladed rotor with clamped blades and flexible hub.

Further, the dynamic response behaviour of the RTG rotor (without aerodynamic forces) in the two-bladed configuration is assessed in terms of intersections found in the frequency diagram between the rotor eigenfrequencies and the rising lines of the first and second rotor harmonics representing 1/rev and 2/rev. For the two-bladed rotor, forced excitation from rotor unbalance is expected for 1/rev (red line) and from the fundamental harmonic of the blade passage frequency for 2/rev (green line). Intersections give those rotational frequencies for which an increased vibratory level is expected and which have to be avoided in operation.

Dynamic stability is judged with the according damping diagram in terms of negative damping values for which instability due to ground resonance is indicated. For the design of the RTG rotor a nominal rotor speed of 50 Hz and a maximum value of 65 Hz in over-speed has to be considered. Attached simulation results in Figure 9 and Figure 10 are gained from the application of linearization features in combination with the eigenvalue solver in MBS SIMPACK and show the development of the rotor frequencies and critical damping of the modes versus rotor speed for the studied dynamic systems. They comprise the rotor configurations of clamped blades with flexible hub as well as articulated blades with lead-lag hinge and rigid hub. The application for the two-bladed RTG rotor with clamped blades shows dynamic stability of the rotor (critical damping ≥ 0.0, zero structural damping) and thus, no sign of ground resonance is present. In contrast, the rotor with lead-lag hinges reaches a minimum damping value of -0.16 % and thus, is instable.

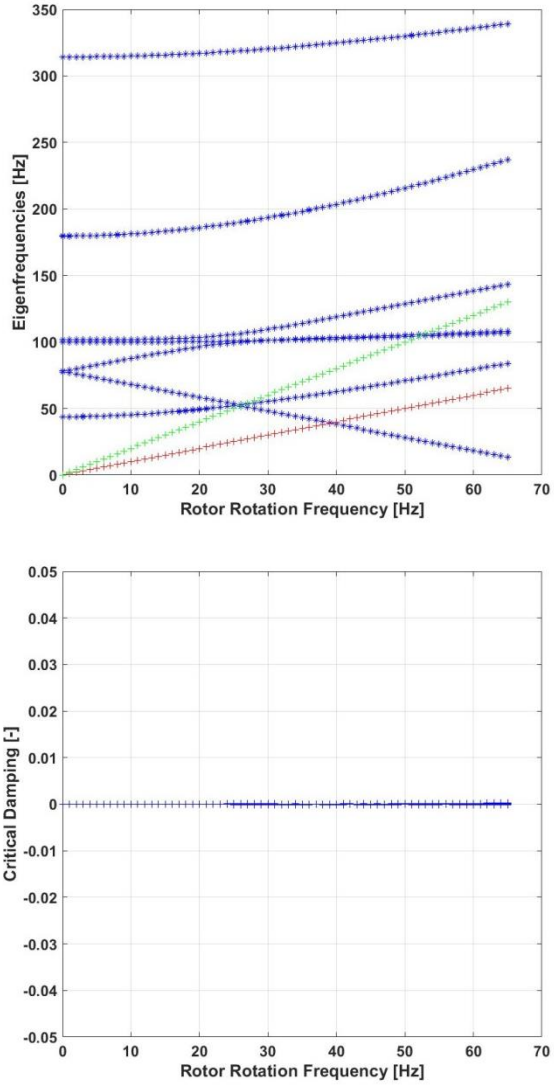

Figure 9. Rotor frequencies and damping for the dynamic model (2 clamped blades with flexible hub).

Presented at 44th European Rotorcraft Forum, Delft, The Netherlands, 19-20 September, 2018
This work is licensed under the Creative Commons Attribution International License (CC BY). Copyright © 2018 by author(s).

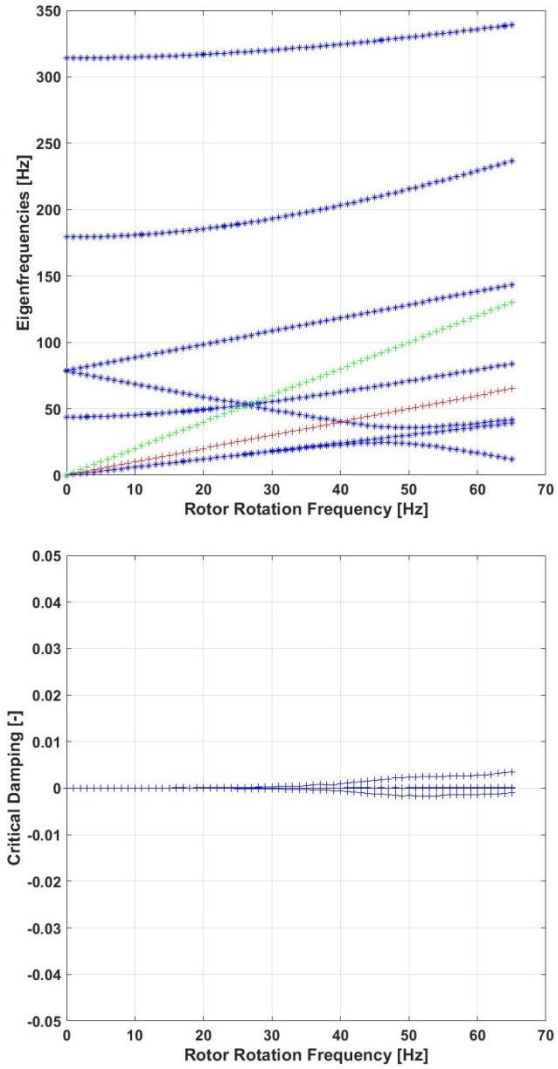

Figure 10. Rotor frequencies and damping for the dynamic model (2 articulated blades with lead-lag hinge).

Changing the two- into a four-bladed rotor, two major differences are found with the dynamic properties. First, the non-rotating four-bladed rotor shows the pairwise appearance of "double" symmetric and antisymmetric eigenforms of the elastic rotor blades (named: sym / anti) which are related now to the motion contributions of two pairs of opposite blades. Second, the natural frequencies of the two whirl modes (named: W-fwd / W-bwd) decrease by around 3.3 Hz for the non-rotating case due to the mass growth which is given by two additional rotor blades and their connecting parts to the rotor hub. This can lead to an increased forced vibration level or rotor instability in unfavourable cases and needs to be considered. With rotation, similar changes in eigenfrequencies of the rotor blades and whirl motion are computed (see Table 3 and compare to Table 2) as found before with the clamped two-bladed rotor. According natural frequencies of the symmetric and antisymmetric blade modes remain more or less unaltered.

Mode No.	0 Hz Rotor Speed	50 Hz Rotor Speed
1 / 2	F1-anti / 43.77 Hz	F1-anti / 70.78 Hz
3 / 4	F1-sym / 43.81 Hz	F1-sym / 70.79 Hz
5	W-bwd / 74.54 Hz	W-bwd / 25.06 Hz
6	W-fwd / 74.56 Hz	W-fwd / 125.67 Hz
7 / 8	L1-anti / 99.60 Hz	L1-anti / 103.26 Hz
9 / 10	L1-sym / 101.22 Hz	L1-sym / 103.03 Hz 105.44 Hz
11 / 12	F2-sym / 179.59 Hz	F2-sym / 215.57 Hz
13 / 14	F2-anti / 179.64 Hz	F2-anti / 215.58 Hz 215.63 Hz
15 / 16	T1-sym / 314.21 Hz	T1-sym / 329.94 Hz
17 / 18	T1-anti / 314.21 Hz	T1-anti / 329.98 Hz
(F = flap mode / L = lag mode / T = torsion mode / W = whirl)		

Table 3: Natural frequencies of four-bladed rotor with clamped blades and flexible hub.

For the four-bladed configuration, the dynamic response behaviour of the RTG rotor (as for the two-bladed rotor here without aerodynamic forces) is assessed for intersections in the frequency diagram between rotor eigenfrequencies and rotor harmonics of 1/rev, 2/rev and in addition 4/rev. Forced excitation from rotor unbalance is possible for 1/rev (red line), from track error for 2/rev (red line) and from fundamental harmonic of the blade passage frequency for 4/rev (green line). The intersections give the rotational speeds for which an increased vibratory level is possible and which need to be avoided. Since the RTG rotor is operated in axial flight condition, excitation related to blade track error with 2/rev is expected to be minor for the four-bladed configuration. Again, the assessment of dynamic stability for rotor speeds up to 65 Hz does not indicate instability due to ground resonance (critical damping ≥ 0.0, zero structural damping) for the four-bladed RTG rotor with clamped rotor blades, whilst the rotor equipped with lead-lag hinges reaches a minimum damping value of -0.22 % and is instable. According simulation results are depicted in Figure 11 and Figure 12, respectively.

Presented at 44th European Rotorcraft Forum, Delft, The Netherlands, 19-20 September, 2018
This work is licensed under the Creative Commons Attribution International License (CC BY). Copyright © 2018 by author(s).

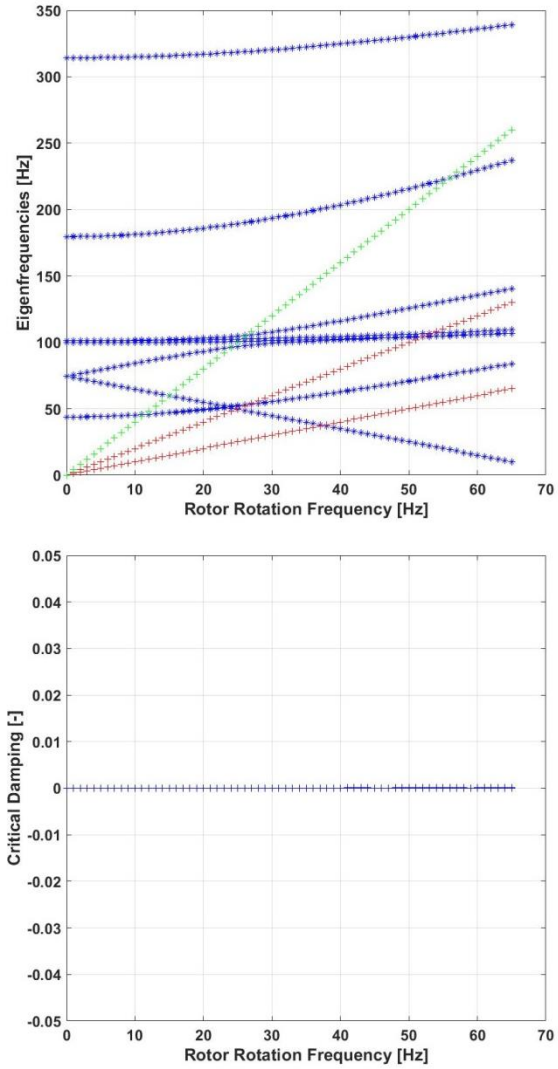

Figure 11. Rotor frequencies and damping for the dynamic model (4 clamped blades with flexible hub).

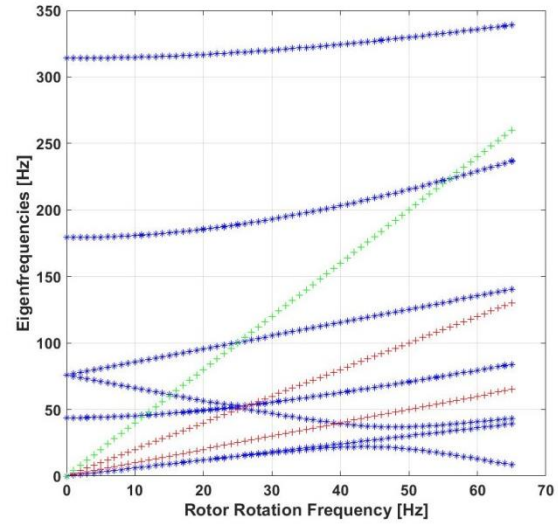

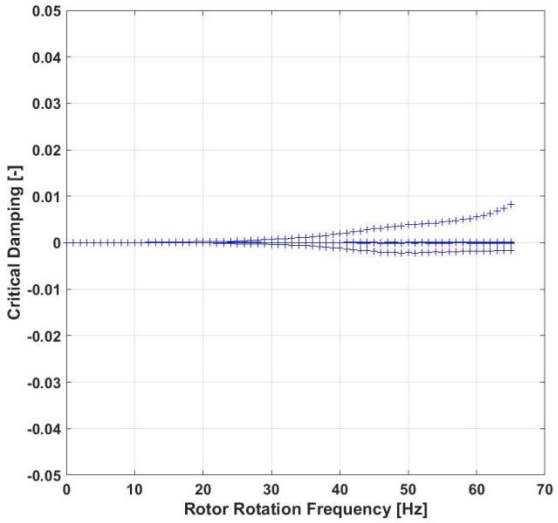

Figure 12. Rotor frequencies and damping for the dynamic model (4 articulated blades with lead-lag hinge).

3.3. Aeroelastic Simulation Results

Aeroelastic results related to the prediction of forced vibration and flutter stability using the unsteady aerodynamic model based on Wagner's function can be gained from the application of linearization features when symmetric axial inflow conditions are assumed and thus, the system matrices remain time invariant. This is valid for the RTG test rig where no additional in-plane velocity component is present, since it is being considered as a "main rotor in axial flight". Similar to the dynamic analyses, the aeroelastic response behaviour of the RTG rotor is assessed in terms of intersections found in the frequency diagram with the rotor harmonics of 1/rev and 2/rev for the two-bladed configuration. For the four-bladed rotor, also 4/rev needs to be taken into account. Intersections give those rotational speeds for which an increased vibratory level is expected, whilst stability is assessed with the according damping diagram in terms of negative damping values for which instability due to rotor blade and rotor flutter is anticipated.

For the safe operation, a nominal rotor speed of 50 Hz and a maximum value of 65 Hz in over-speed is considered. The corresponding results for the two-bladed rotor in Figure 13 and Figure 14 are gained from the application of linearization features in combination with the eigenvalue solver in MBS SIMPACK and show the rotor frequencies and critical damping of the modes versus rotor speed for the aeroelastic model. Except for the RTG rotor configuration with articulated blades at zero rotor speed, all the plotted eigenvalues of zero frequency are of aerodynamic nature and represent the aerodynamic lag states. Here, the

Presented at 44th European Rotorcraft Forum, Delft, The Netherlands, 19-20 September, 2018
This work is licensed under the Creative Commons Attribution International License (CC BY). Copyright © 2018 by author(s).

rotor setup with clamped blades and flexible hub as well as the setup with lead-lag hinges and rigid hub are turning into an undamped and thus, instable system (critical damping < 0.0).

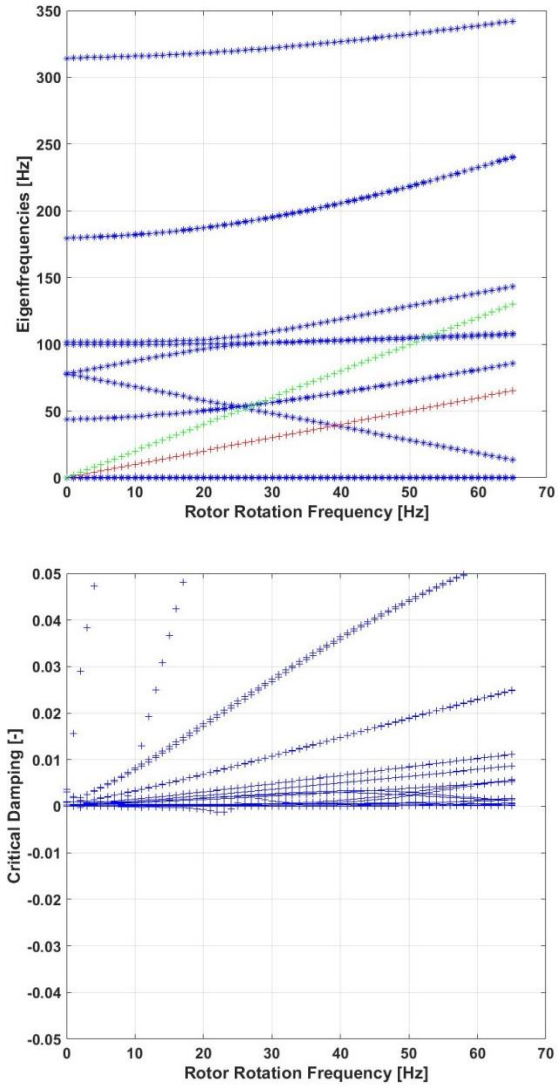

Figure 13. Rotor frequencies and damping for the aeroelastic model (2 clamped blades with flexible hub).

Flutter onset is found for the critical rotational speeds of 20 Hz and 19 Hz, respectively. A small hump mode develops for both rotor setups. According minimum damping values of -0.12 % and -0.09 % show only very small values and are reached for a rotor speed of around 23 Hz. The related flutter mechanism is the same for both rotor setups and shows major contributions from the backward whirl mode W-bwd as well as the first flap bending modes F1-sym and F1-anti (see Table 2). The frequency of the whirl mode at minimum damping is found with 55.15 Hz for the setup with clamped and 56.07 Hz with articulated rotor blades, respectively.

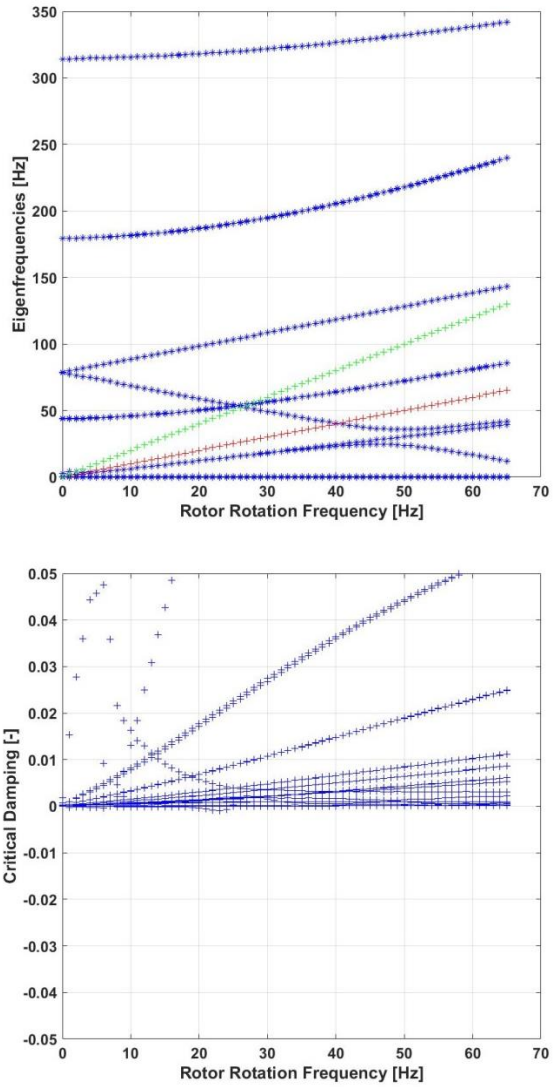

Figure 14. Rotor frequencies and damping for the aeroelastic model (2 articulated blades with lead-lag hinge).

For the four-bladed configuration, the aeroelastic response behaviour of the RTG rotor is assessed for intersections in the frequency diagram between rotor eigenfrequencies and rotor harmonics of 1/rev (red), 2/rev (red) and in addition 4/rev (green) due to the changed blade number. The intersections give the rotational speeds for which an increased vibratory level is possible and which need to be avoided in operation. Here, the assessment of aeroelastic stability for rotor speeds up to 65 Hz does not indicate instability due to flutter (critical damping ≥

Presented at 44th European Rotorcraft Forum, Delft, The Netherlands, 19-20 September, 2018
This work is licensed under the Creative Commons Attribution International License (CC BY). Copyright © 2018 by author(s).

0.0, zero structural damping) for the RTG with clamped and articulated rotor blades. According simulation results are depicted in Figure 15 and Figure 16, respectively.

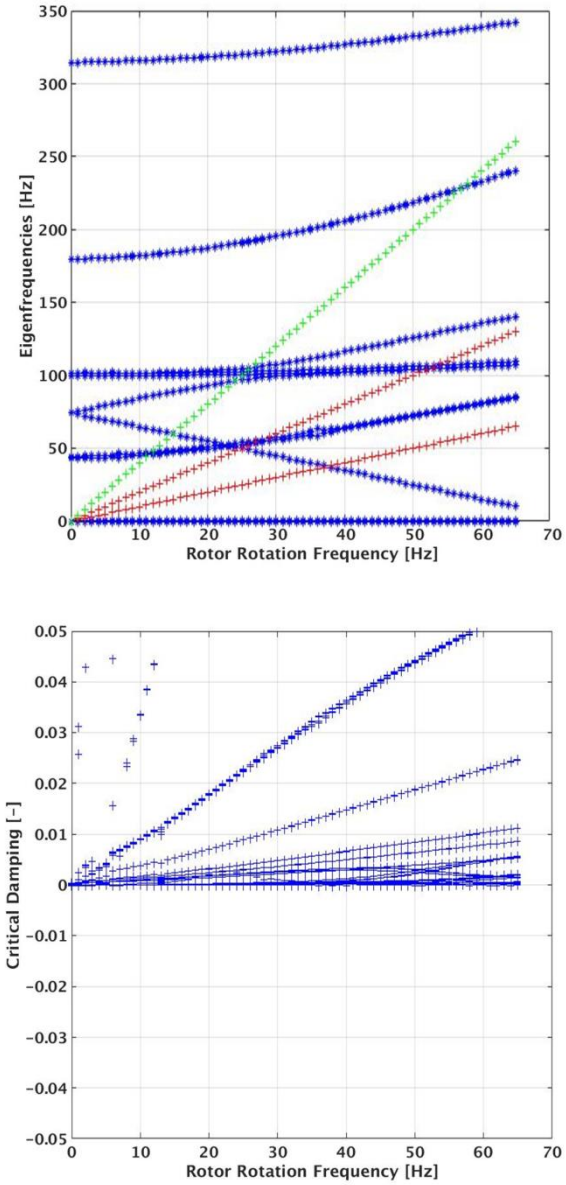

Figure 15. Rotor frequencies and damping for the aeroelastic model (4 clamped blades with flexible hub).

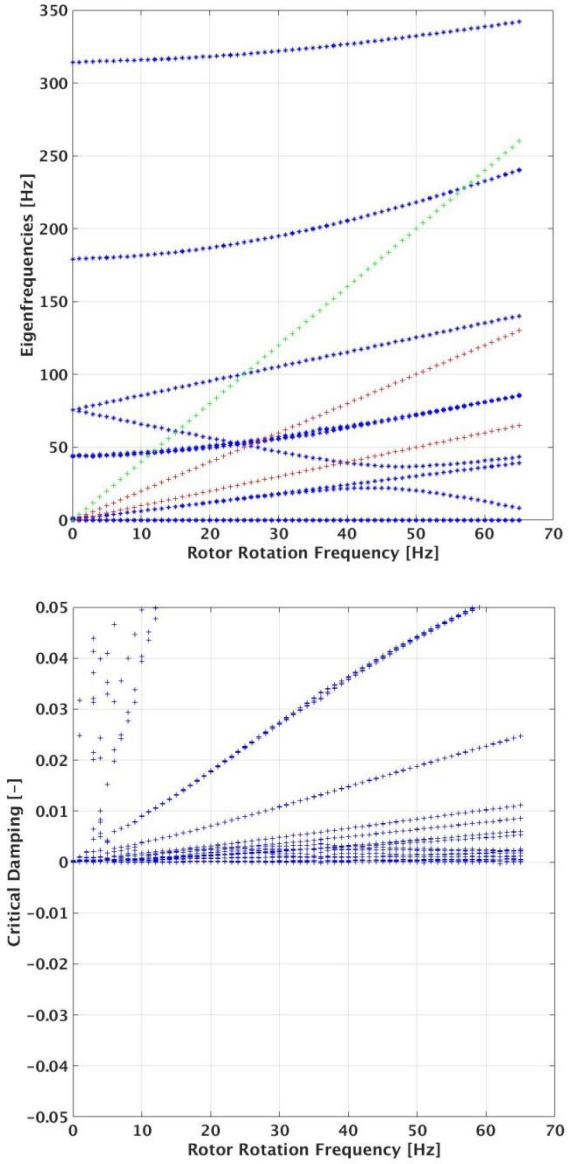

Figure 16. Rotor frequencies and damping for the aeroelastic model (4 articulated blades with lead-lag hinge).

4. CONCLUSIONS AND OUTLOOK

A new double-swept rotor blade setup has been assessed in frequency domain for both, dynamic stability in terms of ground resonance and aeroelastic stability related to rotor blade and rotor flutter. For the aeroelastic analyses, the multibody model was tightly-coupled with an unsteady aerodynamic model based on Wagner's function and related enhancements for the general motion of an airfoil section considering heave and pitch motion.

Numerical results for the two- and four-bladed rotor state the dynamic stability of the rotor test rig for the rotor setup with clamped blades and

Presented at 44th European Rotorcraft Forum, Delft, The Netherlands, 19-20 September, 2018
This work is licensed under the Creative Commons Attribution International License (CC BY). Copyright © 2018 by author(s).

flexible hub in the planned rotor speed range up to 65 Hz. The setup using articulated blades with lead-lag hinges shows minimum damping values of -0.2 % indicating instability at low scale starting from a rotor frequency of 30 Hz. Since the simulation does not consider a lead-lag damper, the introduction of additional lead-lag damping will secure safe operation. Aeroelastic stability results show a “mini-hump” in the damping curves for the two-bladed rotor which is instable for rotor speeds between 19 Hz and 25 Hz for both rotor setups. A minimum damping value of -0.12 % is obtained and the related flutter mechanism shows major contributions from the backward whirl mode and the first flap bending modes. Instability is indicated at very low scale, but needs to be taken into account. Here, the analyses do not consider structural damping and thus, the common magnitude of structural damping will contribute to the mitigation of this minor flutter instability. In contrast, the aeroelastic results of the four-bladed rotor configurations do not show flutter. In comparison to the two-bladed rotor, the natural frequencies of the two whirl modes decrease by around 3 Hz due to the mass growth given by the two additional rotor blades and their connecting parts to the rotor hub. Obviously, this frequency decrease has major impact on the flutter onset.

The presented numerical approach assumes a symmetric rotor with time invariant system matrices as found in axial flight to allow a stability assessment in frequency domain based on extracted eigenvalues using the solver in the multibody software. Further improvement of the used indicial aerodynamics beyond Wagner’s function is currently being prepared to consider additional inflow effects. Finally, the extension of capabilities for rotor blades in forward flight requires the consideration of the stability assessment for time-periodic systems.

5. ACKNOWLEDGEMENT

The authors want to thank their former colleague Mr. Alireza Rezaeian who supported the mentioned GVT and contributed to the setup of the MBS model in an early phase of the project.

6. REFERENCES

[1] Schwermer T, Richter K, Raffel M. “Development of a Rotor Test Facility for the Investigation of Dynamic Stall”, Notes on Numerical Fluid Mechanics and Multidisciplinary Design New Results in Numerical and Experimental Fluid Mechanics X, Springer International Publishing, Switzerland, 2016.

[2] Arnold J, Waitz S. “Using Multibody Dynamics for the Stability Assessment of a New Rotor Test Rig”, 43rd European Rotorcraft Forum, Milan, 2017.

[3] Morillo J, Singh R, Wasikowski M. “Model Development and Integration of DYMORE at Bell Helicopter”, 64th American Helicopter Society Forum, Montréal, 2008.

[4] Waitz S. “The structural dynamics of a free flying helicopter in MBS- and FEM-analysis”, 39th European Rotorcraft Forum, Moscow, 2013.

[5] Lugner P, Arnold M, Vaculin O (Eds). “Vehicle System Dynamics (Special issue in memory Professor Willi Kortüm)”, Vol. 41, No. 5, 2004.

[6] http://www.simpack.com

[7] Fung Y.C. *An Introduction to the Theory of Aeroelasticity*. Dover Publications Inc, New York, 1993, Chapter 6.

[8] Schwertassek R, Wallrapp O. *Dynamik flexibler Mehrkörpersysteme*. Vieweg, 1999.

[9] Wallrapp O. “Standardization of Flexible Body Modeling in Multibody System Codes, Part I: Definition of Standard Input Data”, Mechanics of Structures and Machines, 22(3), pp. 283-304, 1994.

[10] Wagner H. “Über die Entstehung des dynamischen Auftriebes von Tragflügeln“, Zeitschrift für angewandte Mathematik und Mechanik, Band 5, Heft 1, 1925.

[11] Arnold J. “Flutter Assessment of a Rotor Blade with Innovative Layout in Hover using Indicial Aerodynamics”, 72nd American Helicopter Society Forum, West Palm Beach, Florida, 2016.

[12] Rezaeian A. “Whirl flutter analysis of a wind tunnel model using multidisciplinary simulation and multibody dynamics”, Proc 37th European Rotorcraft Forum, Gallarate, 2011.

[13] Krüger W.R. “Multibody analysis of whirl flutter stability on a tiltrotor wind tunnel model”, Proceedings of the Institution of Mechanical Engineers Part K: Journal of

Presented at 44th European Rotorcraft Forum, Delft, The Netherlands, 19-20 September, 2018

This work is licensed under the Creative Commons Attribution International License (CC BY). Copyright © 2018 by author(s).

Multi-body Dynamics, Sage Journals, 2015.

[14] Leishman JG. Modeling of Subsonic Unsteady Aerodynamics for Rotary Wing Applications. AHS Journal, Vol. 35, No. 1, 1990.

[15] Leishman JG. Principles of Helicopter Aerodynamics. Cambridge University Press, New York, 2nd edition, 2000, Chapter 8.

[16] Weerts U, Meister O. “Festigkeitsanalyse fortschrittliche Rotorblätter”, Leichtwerk AG, Report RP-RTG3-00-35-00-001 A01, 2017.

[17] Kage F, Weerts U. “Festigkeitsanalyse des Rotorversuchsstandes”, Leichtwerk AG, Report CR-DLRRT01-0590-001 A.02, 2015.

Presented at 44th European Rotorcraft Forum, Delft, The Netherlands, 19-20 September, 2018

This work is licensed under the Creative Commons Attribution International License (CC BY). Copyright © 2018 by author(s).